 doi:10.20944/preprints201910.0229.v1

Research Article

Identification of Cancer Stem Cell Subpopulations in Head and Neck Metastatic Malignant Melanoma

Vithushiya Yoganandarajah[1], Josie Patel[1], Bede van Schaijik[1], Nicholas Bockett[1], Helen D. Brasch[1], Erin Paterson[1], Dalice Sim[2], Paul F. Davis[1], Imogen Roth[1], Tinte Itinteang[1] and Swee T. Tan[1,3,*]

[1] Gillies McIndoe Research Institute, Wellington, New Zealand; vithushiya@gmail.com (V.Y.); bedevs@gmail.com (B.v.S.); josie.patel@gmri.org.nz (J.P.); nick.bockett@gmri.org.nz (N.B.); helen.brasch@gmri.org.nz (H.D.B); erin.paterson@gmri.org.nz (E.P.); paul.davis@gmri.org.nz (P.F.D); imogen.roth@gmri.org.nz (I.R.); tinte@yahoo.com (T.I.)

[2] Biostatistical Group/Dean's Department, University of Otago, Wellington, New Zealand; simdalice@gmail.com (D.S.)

[3] Wellington Regional Plastic, Maxillofacial and Burns Unit, Hutt Hospital, Wellington, New Zealand.

* Correspondence: swee.tan@gmri.org.nz; Tel.: +64 (0) 4 2820366

Abstract: Cancer stem cells (CSCs) have been identified in many cancer types. This study identified and characterized CSCs in head and neck metastatic malignant melanoma (HNmMM) to regional lymph nodes using induced pluripotent stem cell (iPSC) markers. Immunohistochemical (IHC) staining performed on 20 HNmMM tissue samples demonstrated expression of iPSC markers OCT4, SOX2, KLF4 and c-MYC in all samples while NANOG was expressed at low levels in two samples. Immunofluorescence (IF) staining demonstrated an OCT4+/SOX2+/KLF4+/c-MYC+ CSC subpopulation within the tumor nests (TNs) and another within the peritumoral stroma (PTS) of HNmMM tissues. IF also showed expression of NANOG by some OCT4+/SOX2+/KLF4+/c-MYC+ cells within the TNs in an HNmMM tissue sample that expressed NANOG on IHC staining. *In situ* hybridization (n=6) and reverse-transcription quantitative polymerase chain reaction (n=5) on the HNmMM samples confirmed expression of all five iPSC markers. Western blotting of four primary cell lines derived from four of the 20 HNmMM tissue samples showed expression of SOX2, KLF4, and c-MYC but not OCT4 and NANOG, and three of these cell lines formed tumorspheres *in vitro*. We demonstrate the presence of two putative CSC subpopulations within HNmMM, which may be a novel therapeutic target in the treatment of this aggressive cancer.

Keywords: malignant melanoma, head and neck cancer, cancer stem cell, induced pluripotent stem cell, melanoma metastasis

1. Introduction

In 2018, 287,723 new cases of malignant melanoma (MM) were diagnosed worldwide with a record of 60,712 deaths [1]. MM accounts for 60-80% of deaths from all skin cancers globally with New Zealand and Australia having the highest incidence [2-4]. The 5-year survival of metastatic MM (mMM) is 5-19% depending on the site of the metastasis [2, 5] with an overall median survival of 5-9 months [6-7].

Sentinel lymph node biopsy confers prognostic value and a potential survival advantage for patients with nodal metastases from intermediate-thickness MM who were treated with elective nodal dissection [8-9]. Surgical excision and adjuvant radiotherapy are the mainstay treatment for nodal mMM, with distant metastases requiring chemotherapy and/or immunotherapy [8-9].

MM commonly occurs in the head and neck region [10]. Despite intensive research, the prognosis for head and neck metastatic MM (HNmMM) to regional lymph nodes remains poor with a 5-year survival rate of 17.0-22.6% [11-12]. Stage III and IV disease with metastases to regional lymph nodes as well as to distant organs, such as the lungs, liver, brain, and bones, are associated with 1-year survival rates of 7, 6-7, 6-9, and 2-4 months respectively [13-15].

 doi:10.20944/preprints201910.0229.v1

It has been proposed that the growth and spread of cancer is driven by a subpopulation of cancer cells known as cancer stem cells (CSCs) that are formed following acquisition of mutations in resident physiologically normal embryonic stem cells or progenitor cells [16]. These CSCs are capable of proliferation and self-renewal as well as multi-lineage differentiation into non-tumorigenic cells that are non-proliferative and lack self-renewability [17]. Thus, these CSCs operate in a hierarchical fashion similar to physiological stem cells and contribute to the heterogeneity of the tumor tissue.

Reprogramming of these CSCs requires changes in gene expression that are directly modulated by transcription factors [18]. As such, octamer-binding transcription factor 4 (OCT4), homeobox protein NANOG, Kruppel-like factor 4 (KLF4), sex-determining region Y-box 2 (SOX2), and c-MYC are transcription factors regulating pluripotency and self-renewal of embryonic stem cells and have been shown to reprogram differentiated somatic cells, including melanocytes, into induced pluripotent stem cells (iPSCs) [19-20]. OCT4, NANOG, and c-MYC overexpression has been implicated in metastasis in many cancer types, including MM, in which cells expressing these markers have been shown to confer aggressive motility phenotypes, thus promoting invasiveness [21-23]. Interestingly, OCT4 has also been shown to drive dedifferentiation of MM cells into a CSC-like phenotype with increased tumorigenicity and metastatic capacity [24]. The pro-oncogenic role of KLF4 has been demonstrated in MM cell lines [25], while the tumor initiation and maintenance role of SOX2 has also been well-documented [19]. All, or some of these iPSC markers have been used to identify CSCs in many cancer types including squamous cell carcinoma (SCC) affecting the oral tongue [26], lip [27], buccal mucosa [28] and skin [29], breast cancer [30], glioblastoma [31-32], renal clear cell carcinoma [33], acute myeloid leukemia [34], primary MM [35], metastatic MM (mMM) to the brain [15], rectal cancer [36], primary colon adenocarcinoma [37] and metastatic colon adenocarcinoma to the liver [38].

Despite recent literature showing the presence of CSCs in many cancer types, there is a dearth of information characterizing the presence of CSCs within HNmMM using the iPSC markers. In this study, we aimed to identify and characterize CSCs using the iPSC markers OCT4, NANOG, SOX2, KLF4, and c-MYC in HNmMM to the parotid and/or neck nodes, at both the transcript and protein levels. Here, we demonstrate the presence of an OCT4+/SOX2+/KLF4+/c-MYC+ CSC subpopulation within the tumor nests (TNs) and another within the peritumoral stroma (PTS) in this tumor.

2. Results

2.1. OCT4, NANOG, SOX2, KLF4 and c-MYC proteins are expressed in HNmMM tissue samples

In order to confirm the presence of HNmMM, the slides were stained with hematoxylin and eosin (H&E) that showed TNs, (*arrows*) surrounded by PTS (*arrowheads*) in all 20 tissue samples (Figure 1A). In order to determine the presence of the five iPSC markers, the HNmMM tissue sections underwent immunohistochemical (IHC) staining. This showed nuclear and cytoplasmic expression of OCT4 in the cells within the TNs (Figure 1B, *arrows*) and the PTS (Figure 1B, *arrowheads*). NANOG showed weak cytoplasmic staining in only two of the 20 samples (a representative image of the two is shown in Figure 1C) while SOX2 (Figure 1D), KLF4 (Figure 1E), and c-MYC (Figure 1F) were present in all 20 tissue samples. SOX2 was localized predominantly to the nucleus and occasionally the cytoplasm of the cells within the TNs (Figure 1D, *arrows*) and the cells within the PTS (Figure 1D, *arrowheads*). Ubiquitous cytoplasmic staining of KLF4 was found in the cells within the TNs (Figure 1E, *arrows*), and to a lesser extent, the cells within the PTS (Figure 1E, *arrowheads*), while c-MYC showed focal nuclear staining and moderate cytoplasmic staining of the cells within the TNs (Figure 1F, *arrows*) and the cells within the PTS (Figure 1F, *arrowheads*). In most of the samples NANOG was not detected within the TNs.

 doi:10.20944/preprints201910.0229.v1

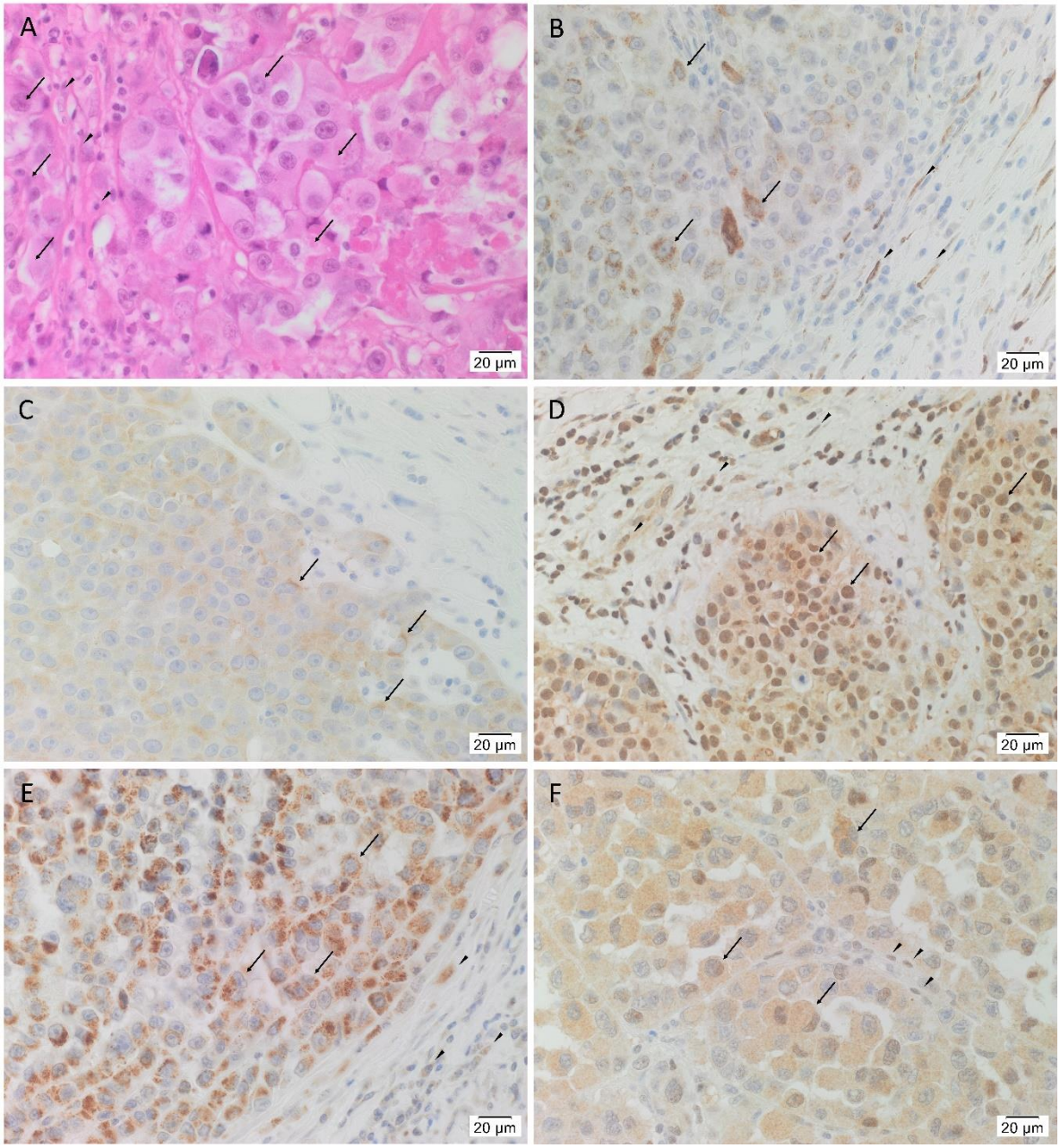

Figure 1. Expression of OCT4, NANOG, SOX2, KLF4, and c-MYC in head and neck metastatic malignant melanoma (HNmMM). Representative hematoxylin and eosin stained section (**A**) and immunohistochemical stained sections (**B**-**F**) of HNmMM demonstrating the tumor organized into tumor nests (TNs, *arrows*) surrounded by the peritumoral stroma (PTS, *arrowheads*). OCT4 (**B**, brown) was expressed on the nucleus and cytoplasm of the cells within the TNs and the cells within the PTS. SOX2 (**D**, brown) was predominantly expressed in the nucleus of the cells within the TNs with some cytoplasmic expression in the cells within the TNs and the cells within the PTS. KLF4 (**E**, brown) was expressed predominantly in the cytoplasm of the cells within the TNs with weak staining in the cells within the PTS. Moderate cytoplasmic and focal nuclear expression of c-MYC (**F**, brown) was present in the cells within the TNs and the cells within the PTS. NANOG (**C**, brown) was expressed in the cytoplasm of the cells within the TNs in two of the 20 tissue samples. Nuclei were counterstained with hematoxylin (**A-F**, blue). Original magnification 400x; n = 20.

Expected staining patterns were demonstrated in the human positive control tissues: seminoma for OCT4 (Figure S1A, brown) and NANOG (Figure S1B, brown), normal skin for SOX2 (Figure S1C,

Preprints (www.preprints.org) | NOT PEER-REVIEWED | Posted: 19 October 2019 doi:10.20944/preprints201910.0229.v1

brown), breast carcinoma for KLF4 (Figure S1D, brown), and normal colon for c-MYC (Figure S1E, brown). The isotype matched antibody provided an appropriate negative control (Figure S1F).

In order to compare the protein expression of different iPSC markers, we performed cell counting analysis on IHC slides of 19 HNmMM samples from the original cohort of 20 patients, excluding one sample that contained dense melanin pigmentation. When comparing the total proportion of positively stained cells within the TNs and PTS for each marker, post hoc statistical analysis demonstrated a hierarchy of expression of these markers with increasing abundance as follows: NANOG < OCT4 < KLF4 < c-MYC < SOX2 (Figure 2). All comparisons were highly statistically significant between markers ($p<0.001$) except for the comparisons between NANOG and OCT4, and between c-MYC and SOX2.

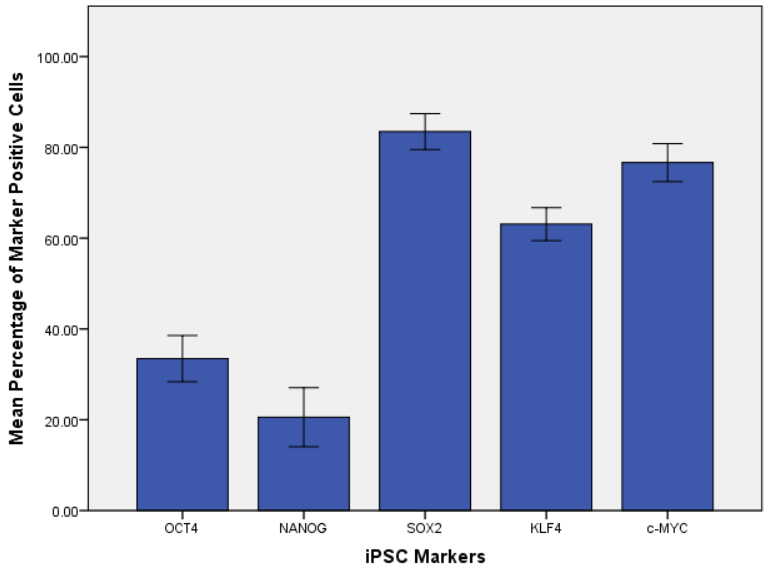

Figure 2. Mean percentage of all positive cells within the tumor nests and the peritumoral stroma of immunohistochemical stained sections of head and neck metastatic malignant melanoma that stained positively for each of the induced pluripotent stem cell markers OCT4, NANOG, SOX2, KLF4, and c-MYC. Error bars represent 95% confidence intervals of the mean. Three replicates from each of the 19 patient tissue samples were used for an Analysis of Variance (ANOVA) thus giving a sample size of 57 for each of the following markers: OCT4, SOX2, KLF4, and c-MYC (n = 57). For NANOG, three technical replicates from each of the two patient tissue samples were used for an ANOVA thus giving a sample size of 6 (n = 6).

2.2. Subpopulations of CSCs expressing OCT4, NANOG, SOX2, KLF4 and c-MYC are present in HNmMM tissue samples

To investigate localization of two iPSC markers simultaneously, immunofluorescence (IF) staining was performed on two representative HNmMM tissue samples. IF staining demonstrated expression of OCT4 (Figure 3A-C, green), SOX2 (Figure 3B&E, red), KLF4 (Figure 3C&F, red) and c-MYC (Figure 3D-F, green) by the cells within the TNs (*thick arrows*) and the PTS (*arrowheads*). NANOG (Figure 3A&D and inset, red) was present in one sample that showed NANOG expression on IHC staining and was absent in the other sample that did not show NANOG expression on IHC staining. OCT4 was expressed on the NANOG+ (Figure 3A and inset, red), the SOX2+ (Figure 3B and inset, red), and the KLF4+ (Figure 3C and inset, red) cells within the TNs and the PTS. c-MYC was also expressed by the NANOG+ (Figure 3D and inset, red), the SOX2+ (Figure 3E and inset, red), and the KLF4+ (Figure 3F and inset, red) cells within the TNs and the PTS. Interestingly, some c-MYC+ (Figure 3D and inset, green) cells within the TNs were NANOG- (Figure 3D, *thin arrows*). Magnified figure insets have been provided to show enlarged views of the corresponding images.

Preprints (www.preprints.org) | NOT PEER-REVIEWED | Posted: 19 October 2019 doi:10.20944/preprints201910.0229.v1

Images of individual stains of the merged images presented in Figure 3 are provided in Figure S2. Minimal to no staining was present on the negative controls (Figure S2M), confirming the specificity of the primary antibodies used.

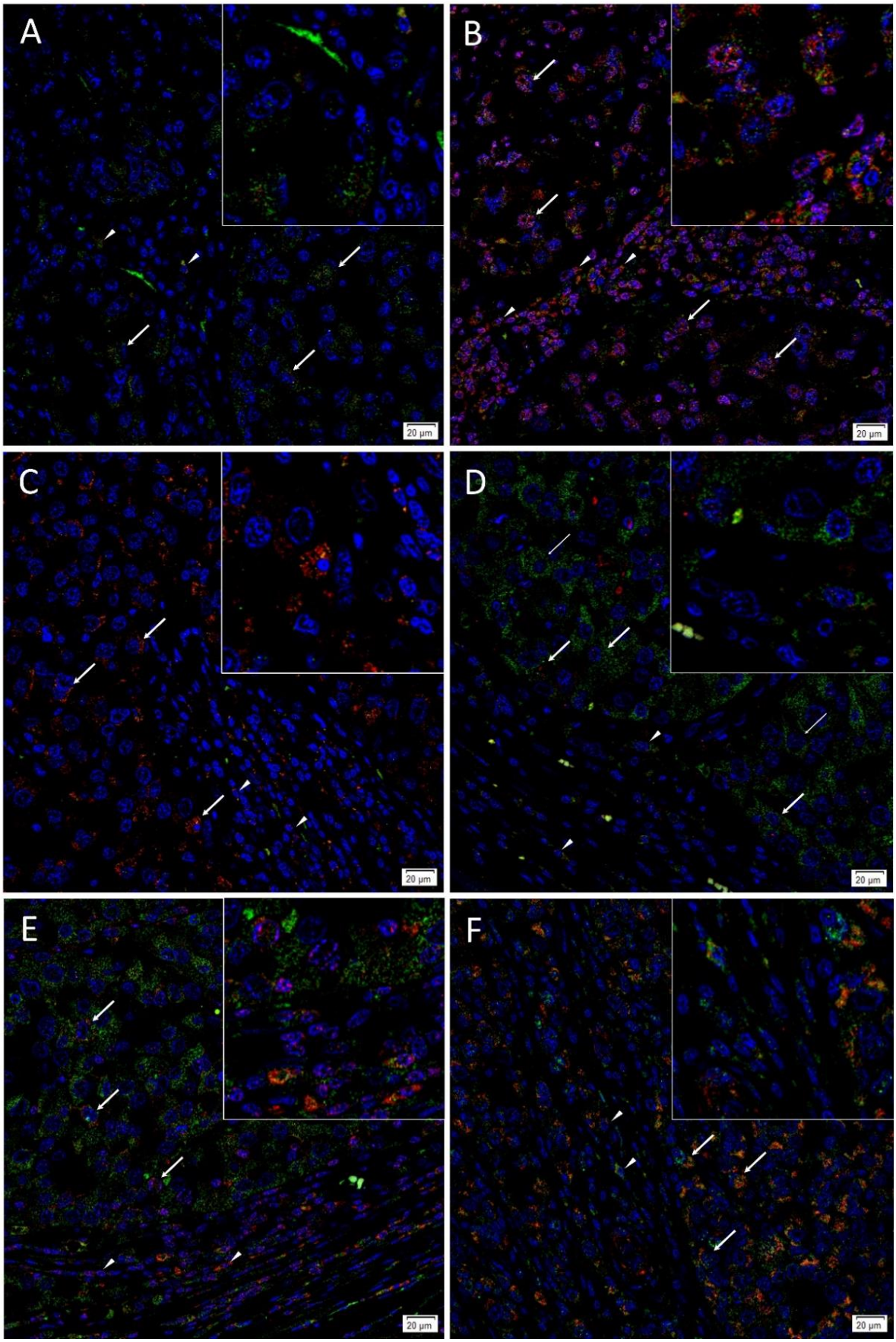

Preprints (www.preprints.org) | NOT PEER-REVIEWED | Posted: 19 October 2019 doi:10.20944/preprints201910.0229.v1

Figure 3. Immunofluorescence stains of head and neck metastatic malignant melanoma tissue samples demonstrating expression of induced pluripotent stem cell markers. Representative sections showing expression of OCT4 (**A-C**, green), SOX2 (**B**, red) and KLF4 (**C**, red) were expressed on the cells within both the tumor nests (TNs, thick arrows) and the peritumoral stroma (PTS, arrowheads). The c-MYC+ [(**D-F**), green] cells within the TNs and the PTS also expressed SOX2 (**E**, red) and KLF (**F**, red). NANOG (**A**, red) was expressed on the OCT4+ (**A**, green) cells within both the TNs (thick arrows) and the PTS (arrowheads), and some cells (thick arrows) and not the others (thin arrows) within the TNs. All slides were counterstained with 4′,6′-diamidino-2-phenylindole (blue). Original magnification 400x; n = 2. The insets show enlarged views of the corresponding images.

2.3. OCT4, NANOG, SOX2, KLF4 and c-MYC mRNA transcripts are expressed in HNmMM tissue and cell samples

In order to determine the transcript expression of the iPSC markers, *in situ* hybridization (ISH) was performed on six HNmMM tissue samples. ISH demonstrated both nuclear and cytoplasmic presence of mRNA for OCT4 (Figure 4A), NANOG (Figure 4B), SOX2 (Figure 4C), KLF4 (Figure 4D) and c-MYC (Figure 4E) in the TNs in all six HNmMM tissue samples. All iPSC markers except NANOG were also expressed in the PTS. The abundance of SOX2 (Figure 4C) and c-MYC (Figure 4E) transcript is in line with the relatively increased expression of these two markers observed at the protein level in cell counting of IHC sections (Figure 2).

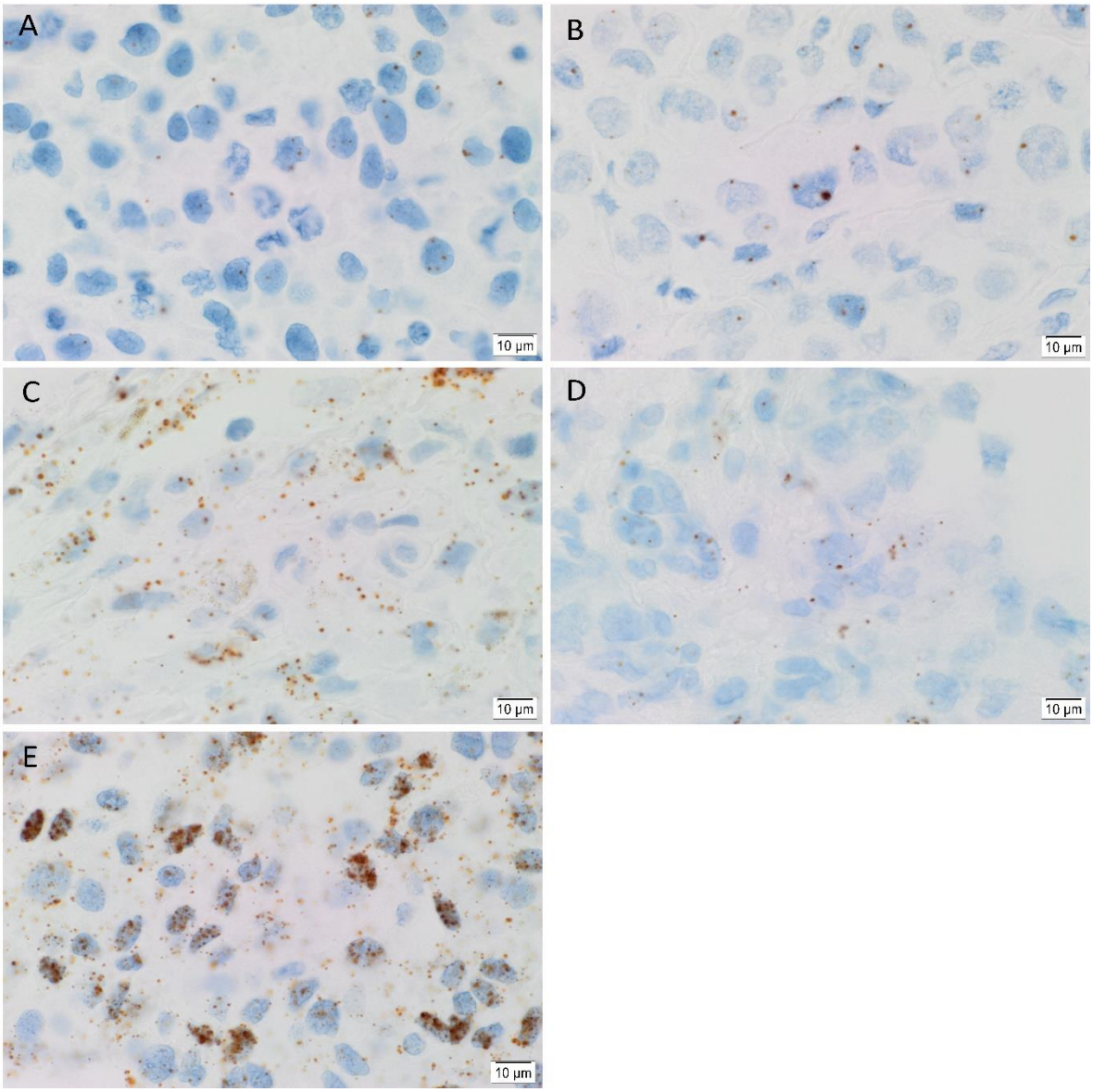

Preprints (www.preprints.org) | NOT PEER-REVIEWED | Posted: 19 October 2019 doi:10.20944/preprints201910.0229.v1

Figure 4. Representative *in situ* hybridization images of head and neck metastatic malignant melanoma tissue samples demonstrating mRNA transcript expression (brown) of induced pluripotent stem cell markers OCT4 (**A**), NANOG (**B**), SOX2 (**C**), KLF4 (**D**) and c-MYC (**E**). Nuclei were counterstained with hematoxylin (**A-E**, blue). Original magnification 1000x; n = 6.

Positive controls demonstrated the expected staining pattern for OCT4 (Figure S3A) and NANOG (Figure S3B) in seminoma, SOX2 (Figure S3C) in normal skin, KLF4 (Figure S3D) in breast carcinoma, and c-MYC (Figure S3E) in normal colon. The negative control (Figure S3F) showed no staining indicating no background activity.

In order to compare the transcript expression of different iPSC markers, we performed cell counting analysis of six ISH stained slides of HNmMM. When comparing the total proportion of positively stained cells within the TNs and the PTS for each marker, post hoc statistical analysis demonstrated a hierarchy of expression of these markers with increasing abundance: KLF4 < SOX2 < OCT4 < NANOG < c-MYC (Figure 5). All comparisons were highly statistically significant between markers ($p<0.001$) except for the comparisons between KLF4, SOX2, and OCT4 which were not statistically significant.

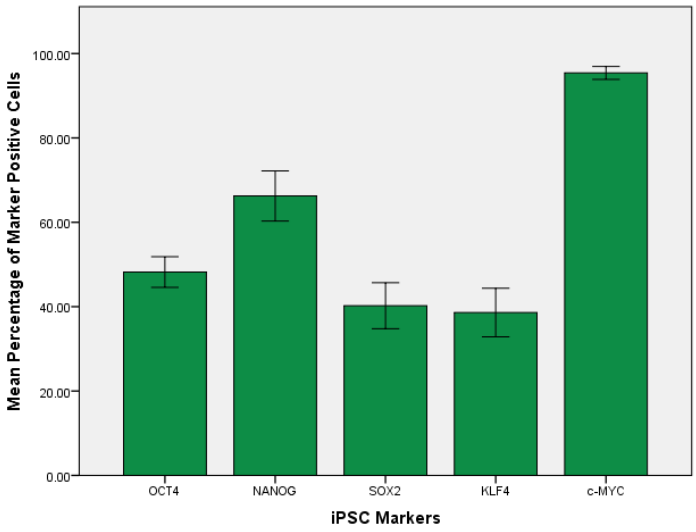

Figure 5. Graph demonstrating mean percentage positive expression of induced pluripotent stem cell markers OCT4, NANOG, SOX2, KLF4, and c-MYC by cells within the tumor nests and the peritumoral stroma on *in situ* hybridization stained sections of head and neck metastatic malignant melanoma. Error bars represent 95% confidence intervals of the mean. Six replicates from each of the six patient tissue samples were used for an Analysis of Variance (ANOVA), thus giving a sample size of 36 for each marker (n = 36).

In order to confirm the transcript expression of iPSC markers, we performed reverse transcriptase quantitative polymerase chain reaction (RT-qPCR) analysis of five snap frozen HNmMM tissue samples and four HNmMM-derived primary cell lines. RT-qPCR analysis of both HNmMM tissue samples (Figure 6A) and HNmMM-derived primary cell lines (Figure 6B) demonstrated expression of all five iPSC markers OCT4, NANOG, SOX2, KLF4, and c-MYC. Specific amplification of the products was demonstrated by electrophoresis of qPCR products on 2% agarose gels (Figure S4A-N). The expected size amplicons were observed, and no products were observed in the no template control (NTC) reactions (Figure S4A-N).

Preprints (www.preprints.org) | NOT PEER-REVIEWED | Posted: 19 October 2019 doi:10.20944/preprints201910.0229.v1

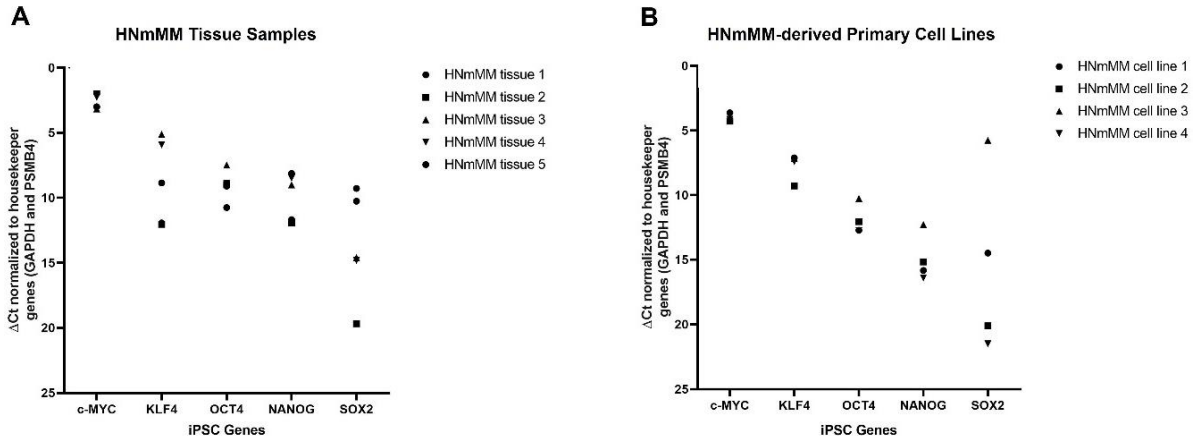

Figure 6. Quantitative transcriptional profiling of induced pluripotent stem cell (iPSC) markers c-MYC, KLF4, OCT4, NANOG, and SOX2. Graphs demonstrating average ΔCT values of triplicate RT-qPCR runs carried out on five snap frozen head and neck metastatic malignant melanoma (HNmMM) tissue samples (**A**) and four HNmMM-derived primary cell lines (**B**) amplifying mRNA transcripts for these iPSC markers. CT values of the iPSC markers were normalized to the housekeeping genes GAPDH and PSMB4 to calculate ΔCT. Note reversed Y-axis for readability.

2.4. SOX2, KLF4 and c-MYC proteins are expressed in the HNmMM-derived primary cell lines

Western blot (WB) analysis of total protein extracts from the four HNmMM-derived primary cell lines showed that OCT4 (Figure 7A, ~39kDa) and NANOG (Figure 7B, ~40kDa) proteins were below detectable levels. SOX2 was detected in one of the four cell lines at ~38kDa, and faint bands were seen in a further two cell lines (Figure 7C). A band of ~40kDa was detected in the NTERA2 cell extract, the difference in size is likely to be due to post-translational modifications. The specificity of this antibody was confirmed using an alternative antibody for SOX2 from a different manufacturer and host species, revealing identical banding patterns (Figure S5A). KLF4 showed specific bands at ~60kDa and, a smaller and likely non-specific band, at ~27kDa (Figure 7D). c-MYC showed a band at ~57kDa in the HNmMM cell extracts as well as in the positive control and a smaller ~40kDa band in two of the HNmMM cell extracts (Figure 7E) which could represent MYC-Nick [39]. α-Tubulin staining confirmed approximately equal total protein loading for the four cell line samples (Figure 7F, ~50kDa).

Densitometric quantification carried out on the HNmMM WB was consistent with the qualitative observation of below detectable levels of OCT4 and NANOG, ubiquitously low SOX2 expression and similar expression levels of KLF4 and c-MYC (Figure S5B&C).

Preprints (www.preprints.org) | NOT PEER-REVIEWED | Posted: 19 October 2019 doi:10.20944/preprints201910.0229.v1

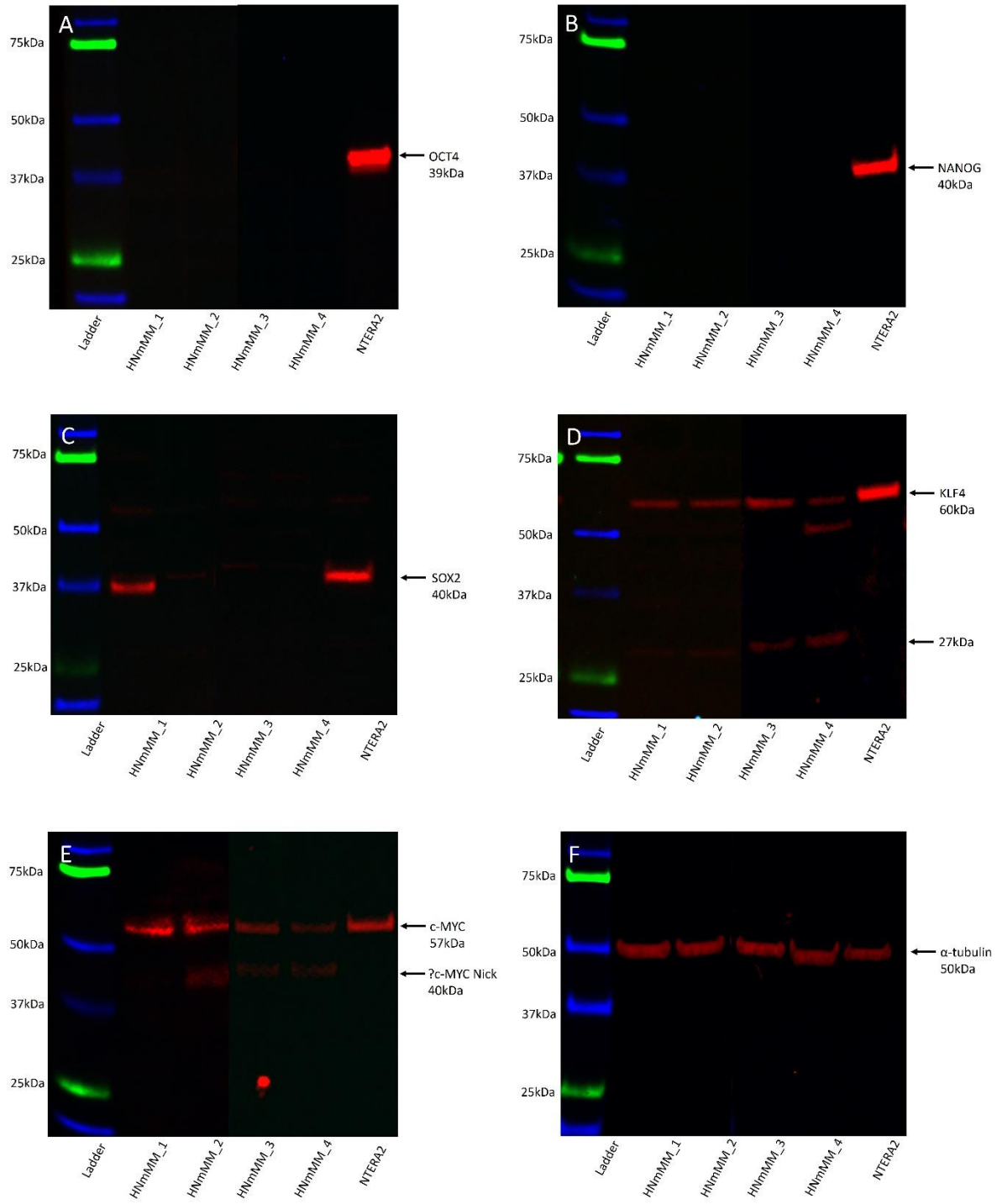

Figure 7. Representative western blot images of total protein extracted from four head and neck metastatic malignant melanoma-derived primary cell lines probed for induced pluripotent stem cell markers. Blots were probed for OCT4 (**A**), NANOG (**B**), SOX2 (**C**), KLF4 (**D**), c-MYC (**E**) and detected with HRP conjugated goat anti-rabbit antibody. α-Tubulin was used as the loading control (**F**) and detected using HRP conjugated mouse IgGκ binding protein. Arrows indicate the presence of the proteins with their expected band sizes.

2.5. HNmMM-derived primary cell lines undergo tumorsphere formation

In order to determine the sphere-forming ability of the CSCs within the HNmMM-derived primary cell lines, we cultured them in tumorsphere media. Three out of four of the cell lines

 doi:10.20944/preprints201910.0229.v1

demonstrated tumorsphere formation (Figure 8A-C, high magnification; Figure S6A-C, low magnification) that met our threshold (spheres that were greater than 50μm in size and more than 50% of spheres measured per field of view were over 50μm [40]) while one cell line formed spheres that did not meet our threshold (Figure 8D, high magnification; Figure S6D, low magnification) in tumorsphere media, providing preliminary evidence that some of the cultured cells may be CSCs.

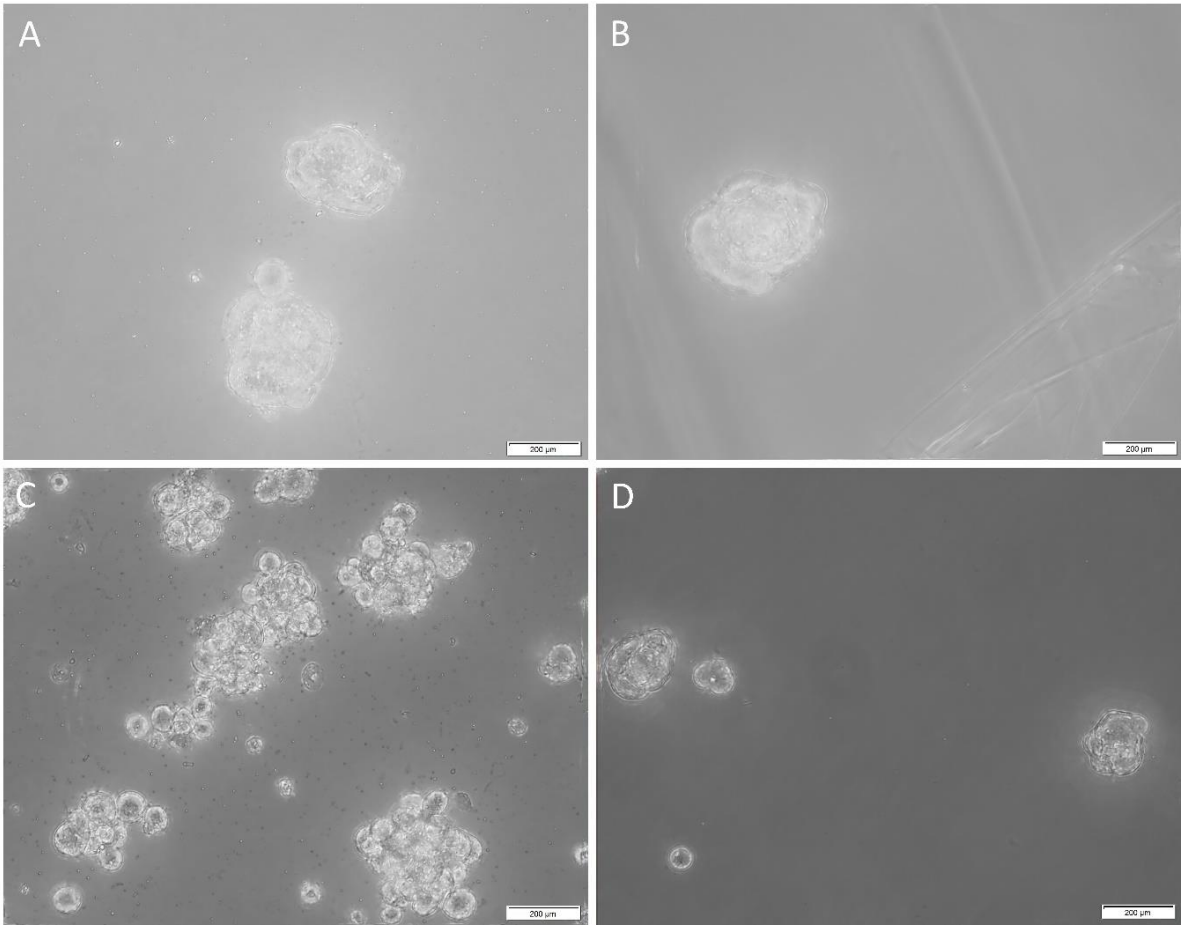

Figure 8. Representative high magnification (40x) images of tumorsphere formation of the three head and neck metastatic malignant melanoma (HNmMM)-derived primary cell lines, averaging 62.7μm in diameter (**A-C**). A representative high magnification (40x) image of one HNmMM-derived primary cell line that did not form spheres, as defined by the tumorsphere criteria in Methods, instead they averaged a diameter of 21μm (**D**).

Taken together, our results show that OCT4, SOX2, KLF4, and c-MYC proteins and transcripts are present within the HNmMM tissue samples and HNmMM-derived primary cell lines. Two out of the 20 HNmMM samples also expressed NANOG. An OCT4+/SOX2+/KLF4+/c-MYC+ subpopulation emerged in two distinct locations within HNmMM: one within the TNs and the other within the PTS. Interestingly, the HNmMM sample that was NANOG+ on IHC staining contained OCT4+/SOX2+/KLF4+/c-MYC+ cells within the TNs on IF staining that were NANOG+ as well as some that were NANOG-. Cell counting analysis of IHC and ISH revealed variable expression of each marker across the tissues. Three out of four HNmMM-derived primary cell lines formed tumorspheres *in vitro* demonstrating the functionality of these cells as CSCs.

3. Discussion

The CSC concept proposes that cancer arises from a pool of cancer stem cells that can give rise to all the cell types within a tumor capable of recreating the heterogeneous phenotype of a tumor

 doi:10.20944/preprints201910.0229.v1

tissue, including producing more tumorigenic CSCs and non-tumorigenic cancer cells. Classically, CSC subpopulations have been defined by their ability to express various markers that have different phenotypic and functional characteristics, even within the same tumour [41]. In this study, we demonstrate the presence of an OCT4+/SOX2+/KLF4+/c-MYC+ CSC subpopulation within the TNs, and another within the PTS in the 20 HNmMM tissue samples analyzed. NANOG expression was detected at low levels, both qualitatively using IHC (Figure 1C) and IF (Figure 3A&D) staining, and quantitatively using cell counting (Figure 2) in two of the 20 samples analyzed. Interestingly, IF staining performed on one of the HNmMM samples that expressed NANOG on IHC staining, showed that some of the OCT4+/SOX2+/KLF4+/c-MYC+ CSCs within the TNs also expressed NANOG.

OCT4 plays a major role in sustaining stem cell self-renewal [42] and causing dedifferentiation of melanoma cells to acquire a CSC phenotype [24]. Our findings are consistent with the expression of OCT4 previously observed in MM, which has been shown to confer chemoresistance and increased motility and invasiveness of melanoma cells [21]. While OCT4 was present in the TNs and the PTS in all 20 HNmMM tissue samples, it was not detected in the four HNmMM-derived primary cell lines examined by WB. This may be attributed to the relatively low levels of the protein in the cell lines compared to the tissues and/or sampling bias. With respect to the observed subcellular localization of OCT4, previous studies have shown that its localization is insignificant in relation to tumorigenesis, as long as nuclear processing is maintained [43].

NANOG protein expression was not detected in 18 out of 20 HNmMM tissue samples by IHC staining (not shown) and in both HNmMM-derived primary cell lines by WB. The low cytoplasmic expression by cells within the TNs of only two of the 20 IHC-stained samples along with sparse expression on the c-MYC+ cells within the TNs demonstrated by IF staining reflects the dispensability of NANOG in the generation of iPSCs [44-45] and perhaps, its dispensability in CSC formation. Interestingly, NANOG was detected by ISH within both the nucleus and cytoplasm of the cells within the TNs, and by RT-qPCR. Possible reasons for this include a delay in translation of NANOG, perhaps due to the transitioning nature of these CSCs, perhaps following differentiation as the maturation, exportation and translation of mRNA is a time-intensive process [46-47]. While known to maintain pluripotency, the function of subcellular localization of NANOG in iPSCs remains unclear [43].

SOX2 expression observed in both the nucleus and the cytoplasm of the cells within the TNs and the PTS of HNmMM tissue samples and its presence in HNmMM-derived primary cell lines may be associated with CSC maintenance and tumor growth [19].

Interestingly, WB analysis for both SOX2 and KLF4 showed smaller bands at 27kDa that appeared to be non-specific as evidenced by their presence in IgG isotype-matched controls. It is likely that these could also represent degradation products of the proteins given their abundant expression in the positive control. The two bands representing SOX2 at 39-43kDa in the NTERA2 cells are likely to be due to post-translational modifications occurring within the cell line [48-49]. Our findings show both a nuclear and cytoplasmic localization of SOX2 and this is supported in the literature where both a nuclear and cytoplasmic role for SOX2 has been described in CSC formation [43].

Abundant c-MYC expression in MM is associated with immune evasion and tumor invasiveness [50], thus its association with poor prognosis and survival [23]. We have observed consistently high cytoplasmic and moderate nuclear expression of c-MYC in the cells within the TNs and the PTS of HNmMM by IHC staining and ISH. This is consistent with c-MYC overexpression observed in most other human malignancies including ocular MM [51] and malignant testicular teratoma [52]. This suggests that while c-MYC expression is mostly cytoplasmic in cancer [43], either nuclear or cytoplasmic expression of c-MYC may contribute to tumorigenesis [43].

Our studies also reveal that the majority of the HNmMM-derived primary cell lines cultured with tumorsphere media formulations *in vitro* succeeded in the isolation and passaging of non-adherent HNmMM tumorspheres thus reflecting the functional capacity of CSCs *in vitro* [53], reminiscent of 'cancer neurospheres' from human glioblastoma multiforme [54]. Further *in vitro* functional research including serial passaging of these HNmMM tumorspheres is needed (as this was

 doi:10.20944/preprints201910.0229.v1

only one passage) to substantiate our findings, and assess multi-lineage (adipogenic, osteogenic, mesenchymal etc) differentiation, another hallmark of cells with stem cell properties [16].

The demonstration of an OCT4+/SOX2+/KLF4+/c-MYC+ CSC subpopulation within the TNs, and another within the PTS of HNmMM in this study is novel. This is important as the two putative CSC subpopulations identified are both OCT4+/SOX2+/KLF4+/c-MYC+ and therefore, may indicate an interaction between the TNs and the PTS in promoting tumor growth [55], although these two subpopulations are distinct from one another, each playing a role in tumorigenesis. However, this is beyond the scope of this study. Future studies with further *in vitro* and *in vivo* functional work are needed to conclusively determine the characteristics of these CSC subpopulations.

Like normal tissues, tumors consist of heterogeneous cell populations that vary due to their apparent state of differentiation [56]. This phenotypic and functional diversity exhibited by CSC subpopulations has been noted in not only the same type of human cancer but also in different subpopulations of CSCs that vary from patient to patient [41] thus giving rise to the idea of intratumoral heterogeneity [57]. This idea of heterogeneity within CSCs extends beyond tumorigenesis to comprise epigenetic, local environmental and genetic differences that could have implications for targeted therapy [58]. This concept is particularly evident in our study where the abundance of iPSC markers within HNmMM is variable using different methods. Comparing expression of these markers in HNmMM tissue, we find that the level of expression of NANOG was the least abundant in IHC staining (Figure 2) compared to the relatively high levels of expression in ISH (Figure 5) and RT-qPCR (Figure 6A). SOX2, on the other hand, was the most abundant on IHC staining (Figure 2) with low expression levels detected by ISH (Figure 5) and RT-qPCR (Figure 6A) in the tissue samples. In contrast, the expression of c-MYC was abundant in HNmMM tissue across IHC staining (Figure 2), ISH (Figure 5) and RT-qPCR (Figure 6A) analyses. As all the samples were acquired from a single tumor type, MM, with loco-regional metastasis to a particular region in the body (the head and neck lymph nodes), one might expect to see similar expression levels of the markers across different methodologies of detection. However, the statistically significant differences between the iPSC-related factors studied allude to the presence of a potential intratumoral heterogeneity within HNmMM. This is consistent with reports of intratumoral heterogeneity of other melanoma markers observed in animal and cell models of MM [57]. A sub-group of tissue samples from the original cohort used for IHC staining were included for ISH and RT-qPCR analyses. Therefore, we speculate that the expression levels and hierarchy of markers observed in HNmMM tissue may be reflected in IHC analysis while ISH and RT-qPCR may reflect the inherent intratumoral heterogeneity. Given that CSCs in HNmMM demonstrate a unique set of iPSC markers, one way of therapeutically targeting these cells is to identify and localize other CSC characteristics such as the demonstration of components of the renin-angiotensin system (RAS) that can be therapeutically modulated via widely available drugs [59].

CSCs have been shown to express components of the renin-angiotensin system (RAS) in several cancer types including buccal mucosal [60], lip [61], oral tongue [62], and cutaneous squamous cell carcinoma [63], glioblastoma [64], metastatic colon adenocarcinoma to the liver [65] and metastatic MM to the brain [66], thus opening up the possibility of cancer therapy using RAS modulators [59]. The RAS, classically involved in blood pressure and fluid volume regulation, plays a critical role in stem cell maintenance and differentiation [67]. Propanolol, a β-blocker traditionally used to lower blood pressure, has been shown to inhibit tumor growth and has been effective in treating the benign vascular tumor infantile hemangioma [68-69] thus suggesting that it might be re-purposed for cancer treatment [70]. As such, *in vivo* [71-74] and *in vitro* [71, 73] models of MM show a reduction in tumor growth and tumor proliferation, as well as inhibition of metastasis [72] by administration of propranolol. The use of propranolol in a prospective cohort study of non-metastatic MM patients has also been associated with a reduced rate of recurrence [75]. The presence of angiotensin II receptor 1 (ATIIR1), one of the key components of the RAS, has been demonstrated in an *in vivo* mouse model of MM [76]. While the use of propranolol may be beneficial in patients with non-metastatic MM [75], the use of another RAS modulator losartan, an ATIIR1 blocker, has been shown to promote cell proliferation in human melanoma cell lines [77]. Therefore, future work investigating the expression

 doi:10.20944/preprints201910.0229.v1

of components of the RAS by CSCs within HNmMM would be worthwhile to fully elucidate the interactions and potential therapeutic value.

4. Materials and Methods

4.1. HNmMM tissue samples

Tissue samples of HNmMM to the parotid and/or neck nodes of 16 male and 4 female patients aged 47-103 (median, 75) years, with a known primary melanoma tumor in the head and neck region (Table S1), were sourced from the Gillies McIndoe Research Institute Tissue Bank, and used in a study approved by the Central Health and Disabilities Ethics Committee (Ref. 12/CEN/74) with written informed consent from all participants.

4.2. HNmMM-derived primary cell lines

HNmMM-derived primary cell lines were established from four fresh surgically excised HNmMM tissue samples from the original cohort of 20 patients by culturing them within a Matrigel explant prior to extraction of the cells following abundant growth in 24-well plates (Raylab, Auckland, New Zealand). The extracted cells were cultured and passaged in a cell culture media consisting of DMEM (1X) and GlutaMAX-1 (cat#10569-010, Life Technologies) supplemented with 10% fetal bovine serum (cat#10091-148, Life Technologies), 5% mTeSR 1 Complete medium (cat#85850, STEMCELL Technologies, Vancouver, BC, Canada), 1% penicillin-streptomycin (cat#15140122, Life Technologies) and 0.2% gentamycin/amphotericin B (cat#R015-10, Life Technologies). All cultures were maintained in a humidified incubator at 37°C with 5% CO_2. All primary cell lines used for the experiments were at passages 4-5 (RT-qPCR and WB) or 8-9 (tumorsphere formation).

4.3. Histochemical, immunohistochemical and immunofluorescent staining

H&E staining and Melan-A staining were carried out on 4 μm thick formalin-fixed paraffin-embedded (FFPE) sections of all 20 HNmMM tissue samples to confirm the presence and diagnosis of the tumor. Tumors that were negative for Melan-A were stained for S100 protein, an alternate confirmatory IHC stain for melanoma. IHC staining of these sections was then undertaken using the Leica BOND RX™ auto-stainer (Leica Biosystems, Nussloch, Germany). Staining for Melan-A (ready-to-use; cat#PA0233, Leica Biosystems, Newcastle-upon-Tyne, UK), S100 (1:200; cat#330M, Cell Marque, Rocklin, CA, USA), OCT4 (1:30; cat#MRQ-10, Cell Marque), NANOG (1:200; cat#EP225, Cell Marque), SOX2 (1:500; cat#PA1-094, ThermoFisher Scientific, Rockford, IL, USA), KLF4 (1:100; cat#NBP2-24749, Novus Biologicals LLC, Littleton, CO, USA), and c-MYC (1:1000; cat#9E10, Abcam, Cambridge, MA, USA) was performed with 3,3-diaminobenzidine as the chromogen and the antibodies were diluted with BOND™ primary antibody diluent (Leica). All IHC-stained slides were mounted in Surgipath Micromount mounting medium (cat#381017322, Leica).

IF staining was performed on two HNmMM tissue samples from the original cohort of 20 patients. This was performed to demonstrate colocalization of two markers using a combination of VectaFluor Excel anti-rabbit 594 (ready-to use; cat#VEDK-1594, Vector Laboratories, Burlingame, CA, USA) and Alexa Fluor anti-mouse 488 (1:500; cat#A21202, Life Technologies, Carlsbad, CA, USA) to detect combinations that included OCT4 and c-MYC. VectaFluor Excel anti-mouse (ready-to-use; cat#VEDK2488, Vector Laboratories) and Alexa Fluor anti-rabbit 594 (1:500; cat#A21207, Life Technologies) were used to detect combinations that included NANOG, SOX2, and KLF4.

Human tissues used for positive controls for the primary antibodies were seminoma for OCT4 and NANOG, normal skin for SOX2, breast carcinoma for KLF4, and normal colon for c-MYC. A negative antibody control was carried out on one randomly selected HNmMM sample per antibody staining run with staining using either a mouse (ready-to-use; cat#IR750, Dako, Carpinteria, CA, USA) or rabbit (ready-to-use; cat#IR600, Dako) primary antibody isotype-matched control for the IHC staining or a combination for the IF staining.

4.4. In situ hybridization

 doi:10.20944/preprints201910.0229.v1

ISH was carried out on 4 μm thick FFPE sections of six randomly selected HNmMM samples from the original cohort of 20 patients using OCT4 (cat#592868), NANOG (cat#604498), SOX2 (cat#477651), KLF4 (cat#457468) and c-MYC (cat#311768-C2) probes (Advanced Cell Diagnostics, Newark, CA, USA) and detected using RNAscope 2.5LS Reagent Brown Kit (cat#322100, Advanced Cell Diagnostics). Positive control tissue sections were used as for IHC sections. Negative controls were demonstrated on sections of HNmMM using a probe for DapB (cat#3120358, Advanced Cell Diagnostics).

4.5. Image analyses and cell counting

IHC and ISH stained slides were visualized and imaged using an Olympus BX53 microscope fitted with an Olympus SC100 digital camera (Olympus, Tokyo, Japan), and processed with the CellSens 2.0 Software (Olympus).

Representative areas of iPSC marker distributions were selected, captured and counted (both within the TNs and the PTS). For IHC staining, three representative fields of each of the 19 sections were selected and counted at 400x magnification, and for ISH, six fields of view were selected and counted at 1000x magnification, using the Cell Counter program on ImageJ and presented as an average proportion of the total number of positive cells in the total number of fields. One sample out of the original cohort of 20 patients was excluded from counting due to potential confounding effect owing to dense melanin pigmentation.

IF stained images were visualized and captured using an Olympus FV1200 biological confocal laser-scanning microscope (Olympus) and subsequently processed with the cellSens Dimension 1.11 software using 2D deconvolution algorithms (Olympus).

4.6. Reverse transcriptase quantitative polymerase chain reaction

Total RNA was isolated from five snap frozen HNmMM tissue samples and four HNmMM-derived primary cell lines from the original cohort of 20 patients. Approximately 20 mg of tissue was homogenized using the Omni Tissue Homogenizer (Omni TH, Omni International, Kennesaw, GA, USA) and then prepared using the RNeasy Mini Kit (cat#74104, Qiagen). Frozen cell pellets of approximately $5x10^5$ viable cells were prepared using the RNeasy Micro Kit (cat#74004, Qiagen). A DNase digest step was included to remove potentially contaminating genomic DNA (cat#79254, Qiagen). The quantity and quality of the RNA was determined using a NanoDrop 2000 Spectrophotometer (ThermoFisher Scientific). Transcript expression was assessed using the Rotor-Gene Q (Qiagen) and the Rotor-Gene Multiplex RT-PCR Kit (cat#204974, Qiagen). The primer probes used were OCT4 (Hs03005111_g1), NANOG (Hs02387400_g1), SOX2 (Hs01053049_s1), KLF4 (Hs00358836_m1) and c-MYC (Hs00153408_m1; cat#4331182) (ThermoFisher Scientific). Gene expression was normalized against the housekeepers GAPDH (Hs99999905_m1) and PSMB4 (Hs00160598_m1; cat#4331182, ThermoFisher Scientific). Positive controls were demonstrated on NTERA2 cell lines with RNase-free water negative controls being used to confirm no contamination and reverse-transcriptase negative controls included for those primers that may detect genomic DNA. End point PCR amplification product specificity was checked using 2% agarose gel (cat#G402002, ThermoFisher Scientific) electrophoresis using the eGel equipment (cat#G6400, ThermoFisher Scientific) and subsequent imaging using the ChemiDoc MP (Bio-Rad Laboratories).

4.7. Western blotting

Total protein extracts from four HNmMM-derived primary cell lines were resolved by 4-12% one-dimensional polyacrylamide gel electrophoresis (ThermoFisher Scientific) at 20 μg total protein per sample and transferred to polyvinylidene difluoride membranes (ThermoFisher Scientific). The membranes were then probed with the following primary antibodies: OCT4 (1:1000; cat#ab109183, Abcam), NANOG (1:500; cat#ab109250, Abcam), SOX2 (1:500; cat#48-1400, ThermoFisher Scientific), KLF4 (1:1000; cat#NBP2-24749, Novus Biologicals, Centennial, CO, USA), c-MYC (1:1000 cat#ab32072, Abcam) and α-tubulin (1:1000; cat#62204, ThermoFisher Scientific) followed by incubation with an

 doi:10.20944/preprints201910.0229.v1

appropriate secondary antibody, either goat anti-rabbit, horseradish peroxidase (HRP) conjugate (1:1000; cat#ab6721, Abcam) for the five iPSC markers or mouse IgGκ binding protein, HRP conjugate (1:2000; cat#sc516102, Santa Cruz Biotechnology, Dallas, TX, USA) for α-tubulin. HRP-conjugated secondary antibody detection and visualization were performed using Clarity Western enhanced chemiluminescence substrate (Bio-Rad Laboratories) and a ChemiDoc MP imaging System (Bio-Rad Laboratories).

Image Lab 6.0 (Bio-Rad Laboratories) was used to perform densitometric quantification of OCT4, NANOG, SOX2, KLF4, and c-MYC expression, relative to α-tubulin. Single bands that corresponded with the expected size of the respective proteins were used for the analysis.

4.8. In-vitro tumorsphere formation assays

Tumorsphere suspension cultures were developed using four HNmMM-derived primary cell lines. Briefly, $2.5x10^5$ live cells from adherent cultures at passages 8-9 were seeded in 25 mL StemXVivo serum-free tumorsphere media (cat#CCM012, R&D Systems, Minneapolis, MN, USA), as per the manufacturer's protocol in T75 Nunclon™ Sphera™ EasYFlasks (cat#174952, ThermoFisher Scientific) and cells were maintained in a 5% CO_2 incubator at 37°C for up to 10 days, and fed every 3-4 days with the addition of 12.5 mL of media. Cells were then observed under an Olympus CKX53 Microscope (Tokyo, Japan) daily from day three. Three fields of view were captured for each cell line, and from each field of view five representative tumorspheres were identified, and two measurements per sphere-like structure were performed to establish an average sphere size per flask. If the average measurements of the spheres were greater than 50µm in size and more than 50% of spheres measured per field of view were over 50µm, the culture was classified as positive for tumorspheres [40]. This was done to account for samples where only a few cells formed tumorspheres.

4.9. Statistical analysis

Statistical analyses for comparison of the iPSC markers investigated by IHC staining and ISH of the HNmMM tissue samples were undertaken. Two types of analyses were done: a) a Analysis of Variance (ANOVA) using the percentage of marker-positive cells as the dependent variable and the iPSC markers and replicates as independent variables, ignoring the fact that the samples came from the same patient, and the replicates from the same sample and so they are correlated; b) to accommodate these correlations, Generalized Estimating Equations [78] with a linear model that required minimal distributional assumptions were used to test whether the mean levels of the five iPSC markers were different. Given the multiple comparisons being made, post hoc analysis with Bonferroni corrections were performed.

5. Conclusions

Our findings demonstrate the presence of two putative subpopulations of CSCs expressing iPSC markers within the TNs and PTS of HNmMM. This enables us to speculate the plastic nature of the CSC hierarchy, where progenitor subpopulations within a tumorigenic niche may be induced to re-acquire a primitive pluripotent CSC state, with the expression of these iPSC-related factors. While the exact mechanism by which CSCs sustain tumorigenesis in HNmMM is yet to be conclusively ascertained, our novel finding of CSC subpopulations in HNmMM acts as a stepping stone for future research to better understand the regulatory pathways for CSCs that may underscore targeted therapy, and thus improved outcomes for patients with HNmMM.

Supplementary Materials: The following are available online, Figure S1: Representative immunohistochemical stained sections of positive and negative human control tissues for the iPSC markers, Figure S2: Split immunofluorescence stained images of head and neck metastatic malignant melanoma tissue samples for the iPSC markers, Figure S3: Positive and negative controls of *in situ* hybridization stained sections for the five iPSC markers, Figure S4: Reverse-transcriptase quantitative polymerase chain reaction amplification products from HNmMM tissue samples and HNmMM-derived primary cell lines were checked using agarose gel electrophoresis, Figure S5: WB analysis of isotype matched control of SOX2 and densitometric quantification of

the iPSC marker expression from WB analysis, Figure S6: Representative low magnification images of tumorsphere formation in the HNmMM-derived cell lines, Table S1: Demographic data and sites of the metastases of the 20 patients with HNmMM.

Author Contributions: Conceptualization, S.T.T. and T.I.; methodology, B.v.S., N.B., J.P., V.Y., E.P., H.D.B. and D.S.; formal analysis, B.v.S., N.B., J.P., V.Y., E.P., H.D.B., S.T.T. and D.S.; investigation, V.Y., B.v.S., J..P., N.B., E.P. and H.D.B.; resources, S.T.T.; data curation, P.F.D.; writing—original draft preparation, V.Y., T.I. and S.T.T.; writing—review and editing, I.R., P.F.D. and S.T.T; supervision, S.T.T. project administration; S.T.T.; validation, P.F.D. and S.T.T; funding acquisition, S.T.T. All authors commented on and approved the final manuscript.

Funding: This research received no external funding

Acknowledgments: The authors would like to thank Ms. Liz Jones of the Gillies McIndoe Research Institute for her assistance with the H&E, IHC and ISH staining. V.Y. was supported by a summer scholarship from the Deane Endowment Trust.

Conflicts of Interest: The authors declare that the research was conducted in the absence of any commercial or financial relationships that could be construed as a potential conflict of interest. T.I., P.F.D., and S.T.T. are inventors of the patent Cancer Diagnosis and Therapy (United States Patent No. 10281472), provisional patents Cancer Diagnosis and Therapy (PCT/NZ2015/050108) and Cancer Therapeutic (PCT/NZ2018/050006), provisional patent application Novel Pharmaceutical Compositions for Cancer Therapy (US/62/711709).

References

1. *Cancer facts & figures, 2018*; American Cancer Society: Atlanta, 2018.
2. Bandarchi, B.; Jabbari, C.A.; Vedadi, A.; Navab, R. Molecular biology of normal melanocytes and melanoma cells. *J Clin Pathol* **2013,** *66*, 644-648.
3. *Clinical practice guidelines for the management of melanoma in australia and new zealand*; The Cancer Council Australia and Australian Cancer Network, Sydney and New Zealand Guidelines Group: Wellington, 2008.
4. Douglas, R.G.; Shaw, J.H. Melanoma of the head and neck in auckland. *N Z Med J* **1987,** *100*, 584-587.
5. Bhatia, S.; Tykodi, S.S.; Thompson, J.A. Treatment of metastatic melanoma: An overview. *Oncology (Williston Park)* **2009,** *23*, 488-496.
6. Khan, K.H.; Goody, R.B.; Hameed, H.; Jalil, A.; Coyle, V.M.; McAleer, J.J. Metastatic melanoma: A regional review and future directions. *Tumori* **2012,** *98*, 575-580.
7. Sandru, A.; Voinea, S.; Panaitescu, E.; Blidaru, A. Survival rates of patients with metastatic malignant melanoma. *J Med Life* **2014,** *7*, 572-576.
8. Morton, D.L.; F., T.J.; J., A.; Cochran, A.J.; Mozzillo, N.; Elashoff, R.; Essner, R.; Nieweg, O.E.; Roses, D.F.; Hoekstra, H.J.; et al. Sentinel-node biopsy or nodal observation in melanoma. *N Eng J Med* **2006,** *355*, 1307-1317.
9. Morton, D.L.; Thompson, J.F.; Cochran, A.J.; Mozzillo, N.; Nieweg, O.E.; Roses, D.F.; Hoekstra, H.J.; Karakousis, C.P.; Puleo, C.A.; Coventry, B.J.; et al. Final trial report of sentinel-node biopsy versus nodal observation in melanoma. *N Eng J Med* **2014,** *370*, 599-609.
10. Schmalbach, C.E.; Johnson, T.M.; Bradford, C.R. The management of head and neck melanoma. *Curr Probl Surg* **2006,** *43*, 781-835.
11. Wang, B.Y.; Lawson, W.; Robinson, R.A.; Perez-Ordonez, B.; Brandwein, M. Malignant melanomas of the parotid: Comparison of survival for patients with metastases from known vs unknown primary tumor sites. *Arch Otolaryngol Head Neck Surg* **1999,** *125*, 635-639.
12. Pour, M.A.H.; Rad, M.; Zarei, M.R.; Chamani, G. Malignant mucosal melanoma of the head and neck diagnosed in an iranian population over an 11-year period. *Am J Appl Sci* **2009,** *6*, 1467-1472.
13. Elder, D.E.; Thompson, J.F. Malignant melanoma. In *World health organisation classification of tumours—pathology & genetics*, 2nd ed.; Kleihues, P., Sobin, L., Eds.; IARC Press: Lyon, France, 2006; pp 52-79.

14. Tas, F. Metastatic behavior in melanoma: Timing, pattern, survival, and influencing factors. *J Oncol* **2012**, 368-375.
15. Wickremesekera, A.C.; Brasch, H.D.; Lee, V.M.; Davis, P.F.; Woon, K.; Johnson, R.; Tan, S.T.; Itinteang, T. Expression of cancer stem cell markers in metastatic melanoma to the brain. *J Clin Neurosci* **2018,** *60*, 112-116.
16. Reya, T.; Morrison, S.J.; Clarke, M.F.; Weissman, I.L. Stem cells, cancer, and cancer stem cells. *Nature* **2001,** *414*, 105-111.
17. O'Connor, M.L.; Xiang, D.; Shigdar, S.; Macdonald, J.; Li, Y.; Wang, T.; Pu, C.; Wang, Z.; Qiao, L.; Duan, W. Cancer stem cells: A contentious hypothesis now moving forward. *Cancer Letters* **2014,** *344*, 180-187.
18. Chambers, Stuart M.; Studer, L. Cell fate plug and play: Direct reprogramming and induced pluripotency. *Cell* **2011,** *145*, 827-830.
19. Santini, R.; Pietrobono, S.; Pandolfi, S.; Montagnani, V.; D'Amico, M.; Penachioni, J.Y.; Vinci, M.C.; Borgognoni, L.; Stecca, B. Sox2 regulates self-renewal and tumorigenicity of human melanoma-initiating cells. *Oncogene* **2014,** *33*, 4697-4708.
20. Utikal, J.; Maherali, N.; Kulalert, W.; Hochedlinger, K. Sox2 is dispensable for the reprogramming of melanocytes and melanoma cells into induced pluripotent stem cells. *J Cell Sci* **2009,** *122*, 3502.
21. Borrull, A.; Ghislin, S.; Deshayes, F.; Lauriol, J.; lcaide-Loridan, C.; Middendorp, S. Nanog and oct4 overexpression increases motility and transmigration of melanoma cells. *J Cancer Res Clin Oncol* **2012,** *138*, 1145-1154.
22. Lin, X.; Sun, R.; Zhao, X.; Zhu, D.; Zhao, X.; Gu, Q.; Dong, X.; Zhang, D.; Zhang, Y.; Li, Y.; et al. C-myc overexpression drives melanoma metastasis by promoting vasculogenic mimicry via c-myc/snail/bax signaling. *J Mol Med (Berl)* **2017,** *95*, 53-67.
23. Grover, R.; Ross, D.A.; Richman, P.I.; Robinson, B.; Wilson, G.D. C-myc oncogene expression in human melanoma and its relationship with tumour antigenicity. *Eur J Surg Oncol* **1996,** *22*, 342-346.
24. Kumar, S.M.; Liu, S.; Lu, H.; Zhang, H.; Zhang, P.J.; Gimotty, P.A.; Guerra, M.; Guo, W.; Xu, X. Acquired cancer stem cell phenotypes through oct4-mediated dedifferentiation. *Oncogene* **2012,** *31*, 4898-4911.
25. Riverso, M.; Montagnani, V.; Stecca, B. Klf4 is regulated by ras/raf/mek/erk signaling through e2f1 and promotes melanoma cell growth. *Oncogene* **2017,** *36*, 3322-3333.
26. Baillie, R.; Tan, S.T.; Itinteang, T. Cancer stem cells in oral cavity squamous cell carcinoma: A review. *Front Oncol* **2017,** *7*, 112.
27. Ram, R.; Brasch, H.D.; Dunne, J.C.; Davis, P.F.; Tan, S.T.; Itinteang, T. The identification of three cancer stem cell subpopulations within moderately differentiated lip squamous cell carcinoma. *Front Surg* **2017,** *4*, 12.
28. Yu, H.H.; Featherston, T.; Tan, S.T.; Chibnall, A.M.; Brasch, H.D.; Davis, P.F.; Itinteang, T. Characterization of cancer stem cells in moderately differentiated buccal mucosal squamous cell carcinoma. *Front Surg* **2016,** *3*, 46.
29. Koh, S.P.; Brasch, H.D.; de Jongh, J.; Itinteang, T.; Tan, S.T. Cancer stem cell subpopulations in moderately differentiated head and neck cutaneous squamous cell carcinoma. *Heliyon* **2019,** *5*, e02257.
30. Yang, F.; Zhang, J.; Yang, H. Oct4, sox2, and nanog positive expression correlates with poor differentiation, advanced disease stages, and worse overall survival in her2(+) breast cancer patients. *Onco Targets Ther* **2018,** *11*, 7873-7881.
31. Bradshaw, A.R.; Wickremesekera, A.; Brasch, H.D.; Chibnall, A.M.; Davis, P.F.; Tan, S.T.; Itinteang, T. Cancer stem cells in glioblastoma multiforme. *Front Surg* **2016,** *3*, 48.
32. Ray, S.K. The transcription regulator krüppel-like factor 4 and its dual roles of oncogene in glioblastoma and tumor suppressor in neuroblastoma. *For Immunopathol Dis Therap* **2016,** *7*, 127-139.

33. Cane, R.; Kennedy-Smith, A.; Brasch, H.B.; Savage, S.; Marsh, R.W.; Itinteang, T.; Tan, S.T. Characterization of cancer stem cells in renal clear cell carcinoma. *J Stem Cell Regen Biol* **2019,** *5*, 6-15.

34. Picot, T.; Aanei, C.M.; Fayard, A.; Flandrin-Gresta, P.; Tondeur, S.; Gouttenoire, M.; Tavernier-Tardy, E.; Wattel, E.; Guyotat, D.; Campos, L. Expression of embryonic stem cell markers in acute myeloid leukemia. *Tumor Biol* **2017,** *39*, 1010428317716629.

35. Klein, W.M.; Wu, B.P.; Zhao, S.; Wu, H.; Klein-Szanto, A.J.P.; Tahan, S.R. Increased expression of stem cell markers in malignant melanoma. *Mod Pathol* **2007,** *20*, 102-107.

36. You, L.; Guo, X.; Huang, Y. Correlation of cancer stem-cell markers oct4, sox2, and nanog with clinicopathological features and prognosis in operative patients with rectal cancer. *Yonsei Med J* **2018,** *59*, 35-42.

37. Munro, M.J.; Wickremesekera, S.K.; Peng, L.; Marsh, R.W.; Itinteang, T.; Tan, S.T. Cancer stem cell subpopulations in primary colon adenocarcinoma. *PLoS ONE* **2019,** *14*, e0221963.

38. Humphries, H.N.; Wickremesekera, S.K.; Marsh, R.W.; Brasch, H.D.; Mehrotra, S.; Tan, S.T.; Itinteang, T. Characterization of cancer stem cells in colon adenocarcinoma metastasis to the liver. *Front Surg* **2018,** *4*, 76.

39. Conacci-Sorrell, M.; Ngouenet, C.; Eisenman, R.N. Myc-nick: A cytoplasmic cleavage product of myc that promotes alpha-tubulin acetylation and cell differentiation. *Cell* **2010,** *142*, 480-493.

40. Lee, C.H.; Yu, C.C.; Wang, B.Y.; Chang, W.W. Tumorsphere as an effective in vitro platform for screening anti-cancer stem cell drugs. *Oncotarget* **2016,** *7*, 1215-1226.

41. Tang, D.G. Understanding cancer stem cell heterogeneity and plasticity. *Cell Research* **2012,** *22*, 457-472.

42. Hadjimichael, C.; Chanoumidou, K.; Papadopoulou, N.; Arampatzi, P.; Papamatheakis, J.; Kretsovali, A. Common stemness regulators of embryonic and cancer stem cells. *World J Stem Cells* **2015,** *7*, 1150-1184.

43. van Schaijik, B.; Davis, P.F.; Wickremesekera, A.C.; Tan, S.T.; Itinteang, T. Subcellular localisation of the stem cell markers oct4, sox2, nanog, klf4 and c-myc in cancer: A review. *J Clin Path* **2018,** *71*, 88-91.

44. Schwarz, Benjamin A.; Bar-Nur, O.; Silva, José C.R.; Hochedlinger, K. Nanog is dispensable for the generation of induced pluripotent stem cells. *Curr Biol* **2014,** *24*, 347-350.

45. Takahashi, K.; Yamanaka, S. Induction of pluripotent stem cells from mouse embryonic and adult fibroblast cultures by defined factors. *Cell* **2006,** *126*, 663-676.

46. Liu, Y.; Beyer, A.; Aebersold, R. On the dependency of cellular protein levels on mrna abundance. *Cell* **2016,** *165*, 535-550.

47. Schwanhäusser, B.; Busse, D.; Li, N.; Dittmar, G.; Schuchhardt, J.; Wolf, J.; Chen, W.; Selbach, M. Global quantification of mammalian gene expression control. *Nature* **2011,** *473*, 337-342.

48. Perrett, R.M.; Turnpenny, L.; Eckert, J.J.; O'Shea, M.; Sonne, S.B.; Cameron, I.T.; Wilson, D.I.; Meyts, E.R.-D.; Hanley, N.A. The early human germ cell lineage does not express sox2 during in vivo development or upon in vitro culture1. *Biol Reprod* **2008,** *78*, 852-858.

49. Van Hoof, D.; Muñoz, J.; Braam, S.R.; Pinkse, M.W.H.; Linding, R.; Heck, A.J.R.; Mummery, C.L.; Krijgsveld, J. Phosphorylation dynamics during early differentiation of human embryonic stem cells. *Cell Stem Cell* **2009,** *5*, 214-226.

50. Garte, S.J. The c-myc oncogene in tumor progression. *Crit Rev Oncog* **1993,** *4*, 435-449.

51. Royds, J.A.; Sharrard, R.M.; Parsons, M.A.; Lawry, J.; Rees, R.; Cottam, D.; Wagner, B.; Rennie, I.G. C-myc oncogene expression in ocular melanomas. *Graefes Arch Clin Exp Ophthalmol* **1992,** *230*, 366-371.

52. Sikora, K.; Evan, G.; Stewart, J.; Watson, J.V. Detection of the c-myc oncogene product in testicular cancer. *Br J Cancer* **1985,** *52*, 171-176.

53. Weiswald, L.-B.; Bellet, D.; Dangles-Marie, V. Spherical cancer models in tumor biology. *Neoplasia* **2015,** *17*, 1-15.

630 54. Galli, R.; Binda, E.; Orfanelli, U.; Cipelletti, B.; Gritti, A.; De Vitis, S.; Fiocco, R.; Foroni, C.; Dimeco, F.;
631 Vescovi, A. Isolation and characterization of tumorigenic, stem-like neural precursors from human glioblastoma.
632 *Cancer Research* **2004,** *64*, 7011.
633 55. Park, T.S.; Donnenberg, V.S.; Donnenberg, A.D.; Zambidis, E.T.; Zimmerlin, L. Dynamic interactions
634 between cancer stem cells and their stromal partners. *Curr Pathobiol Rep* **2014,** *2*, 41-52.
635 56. Dalerba, P.; Cho, R.W.; Clarke, M.F. Cancer stem cells: Models and concepts. *Annual Review of Medicine* **2007,**
636 *58*, 267-284.
637 57. Grzywa, T.M.; Paskal, W.; Włodarski, P.K. Intratumor and intertumor heterogeneity in melanoma. *Transl*
638 *Oncol* **2017,** *10*, 956-975.
639 58. Hinohara, K.; Polyak, K. Intratumoral heterogeneity: More than just mutations. *Trends in Cell Biology* **2019,**
640 *29*, 569-579.
641 59. Roth, I.M.; Wickremesekera, A.C.; Wickremesekera, S.K.; Davis, P.F.; Tan, S.T. Therapeutic targeting of
642 cancer stem cells via modulation of the renin-angiotensin system. *Front Oncol* **2019,** *9*, 745.
643 60. Featherston, T.; Yu, H.H.; Dunne, J.C.; Chibnall, A.M.; Brasch, H.D.; Davis, P.F.; Tan, S.T.; Itinteang, T.
644 Cancer stem cells in moderately differentiated buccal mucosal squamous cell carcinoma express components of
645 the renin-angiotensin system. *Front Surg* **2016,** *3*.
646 61. Ram, R.S.; Brasch, H.D.; Dunne, J.C.; Davis, P.F.; Tan, S.T.; Itinteang, T. Cancer stem cells in moderately
647 differentiated lip squamous cell carcinoma express components of the renin-angiotensin system. *Front Surg* **2017,**
648 *4*, 30-30.
649 62. Itinteang, T.; Dunne, J.C.; Chibnall, A.M.; Brasch, H.D.; Davis, P.F.; Tan, S.T. Cancer stem cells in
650 moderately differentiated oral tongue squamous cell carcinoma express components of the renin–angiotensin
651 system. *J Clin Pathol* **2016,** *69*, 942.
652 63. Nallaiah, S.; Lee, V.M.Y.; Brasch, H.D.; de Jongh, J.; Schaijik, B.v.; Marsh, R.; Tan, S.T.; Itinteang, T. Cancer
653 stem cells within moderately differentiated head and neck cutaneous squamous cell carcinoma express
654 components of the renin-angiotensin system. *J Plast Reconstr Aesthet Surg* **2019,** *72*, 1484-1493.
655 64. Bradshaw, A.R.; Wickremesekera, A.C.; Brasch, H.D.; Chibnall, A.M.; Davis, P.F.; Tan, S.T.; Itinteang, T.
656 Glioblastoma multiforme mancer stem cells express components of the renin-angiotensin system. *Front Surg*
657 **2016,** *3*.
658 65. Narayanan, A.; Wickremesekera, S.K.; van Schaijik, B.; Marsh, R.W.; Brasch, H.D.; Tan, S.T.; Itinteang, T.
659 Cancer stem cells in liver metastasis from colorectal adenocarcinoma express components of the renin-
660 angiotensin system. *J Cancer Metastasis Treat* **2019,** *5*.
661 66. Wickremesekera, A.C.; Brasch, H.D.; Lee, V.M.; Davis, P.F.; Parker, A.; Koeck, H.; Itinteang, T.; Tan, S.T.
662 Cancer stem cell subpopulations in metastatic melanoma to the brain express components of the renin-
663 angiotensin system. *J Cancer Metastasis Therapy* **2019,** *5*, 62.
664 67. Matsushita, K.; Wu, Y.; Okamoto, Y.; Pratt Richard, E.; Dzau Victor, J. Local renin angiotensin expression
665 regulates human mesenchymal stem cell differentiation to adipocytes. *Hypertension* **2006,** *48*, 1095-1102.
666 68. Léauté-Labrèze, C.; Hoeger, P.; Mazereeuw-Hautier, J.; Guibaud, L.; Baselga, E.; Posiunas, G.; Phillips, R.J.;
667 Caceres, H.; Lopez-Gutierrez, J.C.; Ballona, R.; et al. A randomized, controlled trial of oral propranolol in infantile
668 hemangioma. *N Eng J Med* **2015,** *372*, 735-746.
669 69. Tan, S.T.; Itinteang, T.; Leadbitter, P. Low-dose propranolol for infantile haemangioma. *J Plast Reconstr*
670 *Aesthet Surg* **2011,** *64*, 292-299.
671 70. Pantziarka, P.; Bouche, G.; Sukhatme, V.; Meheus, L.; Rooman, I.; Sukhatme, V.P. Repurposing drugs in
672 oncology (redo)-propranolol as an anti-cancer agent. *Ecancermedicalscience* **2016,** *10*, 680.

673 71. Wrobel, L.J.; Le Gal, F.A. Inhibition of human melanoma growth by a non-cardioselective beta-blocker. *J*
674 *Invest Dermatol* **2015,** *135*, 525-531.
675 72. Jean Wrobel, L.; Bod, L.; Lengagne, R.; Kato, M.; Prévost-Blondel, A.; Le Gal, F.-A. Propranolol induces a
676 favourable shift of anti-tumor immunity in a murine spontaneous model of melanoma. *Oncotarget* **2016,** *7*, 77825-
677 77837.
678 73. Zhou, C.; Chen, X.; Zeng, W.; Peng, C.; Huang, G.; Li, X.a.; Ouyang, Z.; Luo, Y.; Xu, X.; Xu, B.; et al.
679 Propranolol induced g0/g1/s phase arrest and apoptosis in melanoma cells via akt/mapk pathway. *Oncotarget*
680 **2016,** *7*, 68314-68327.
681 74. Maccari, S.; Buoncervello, M.; Rampin, A.; Spada, M.; Macchia, D.; Giordani, L.; Stati, T.; Bearzi, C.;
682 Catalano, L.; Rizzi, R.; et al. Biphasic effects of propranolol on tumour growth in b16f10 melanoma-bearing mice.
683 *Br J Pharmacol* **2017,** *174*, 139-149.
684 75. De Giorgi, V.; Grazzini, M.; Benemei, S.; Marchionni, N.; Botteri, E.; Pennacchioli, E.; Geppetti, P.; Gandini,
685 S. Propranolol for off-label treatment of patients with melanoma: Results from a cohort study. *JAMA Oncol* **2018,**
686 *4*, e172908-e172908.
687 76. Egami, K.; Murohara, T.; Shimada, T.; Sasaki, K.-i.; Shintani, S.; Sugaya, T.; Ishii, M.; Akagi, T.; Ikeda, H.;
688 Matsuishi, T.; et al. Role of host angiotensin ii type 1 receptor in tumor angiogenesis and growth. *J Clin Invest*
689 **2003,** *112*, 67-75.
690 77. Renziehausen, A.; Wang, H.; Rao, B.; Weir, L.; Nigro, C.L.; Lattanzio, L.; Merlano, M.; Vega-Rioja, A.; del
691 Carmen Fernandez-Carranco, M.; Hajji, N.; et al. The renin angiotensin system (ras) mediates bifunctional
692 growth regulation in melanoma and is a novel target for therapeutic intervention. *Oncogene* **2019,** *38*, 2320-2336.
693 78. Hanley, J.A.; Negassa, A.; Edwardes, M.D.; Forrester, J.E. Statistical analysis of correlated data using
694 generalized estimating equations: An orientation. *Am J Epidemiol* **2003,** *157*, 364-375.
695